.

Suppressed antinodal coherence with a single d-wave superconducting gap leads to two energy scales in underdoped cuprates

S. Blanc, Y. Gallais, M. Cazayous, M. A. Measson and A. Sacuto

Laboratoire Matériaux et Phénomènes Quantiques (UMR 7162 CNRS), Université Paris Diderot-Paris 7, Bat. Condorcet, 75205 Paris Cedex 13, France

A. Georges

Centre de Physique Théorique, CNRS, Ecole Polytechnique, 91128 Palaiseau Cedex, France and Collège de France, 11 place Marcelin Berthelot, 75005 Paris, France

G.D. Gu, J.S. Wen and Z.J. Xu

Matter Physics and Materials Science, Brookhaven National Laboratory (BNL), Upton, NY 11973, USA

D. Colson

Service de Physique de l'Etat Condensé, CEA-Saclay, 91191 Gif-sur-Yvette, France

(Dated: April 15, 2010)

Conventional superconductors are characterized by a single energy scale, the superconducting gap, which is proportional to the critical temperature (T_c)[1].

In hole-doped high-T_c copper oxide superconductors, previous experiments [2–6] have established the existence of two distinct energy scales for doping levels below the optimal one. The origin and significance of these two scales are largely unexplained, although they have often been viewed as evidence for two gaps, possibly of distinct physical origins [5–8]. By measuring the temperature dependence of the electronic Raman response of $Bi_2Sr_2CaCu_2O_{8+\delta}$ (Bi-2212) and $HgBa_2CuO_{4+\delta}$ (Hg-1201) crystals with different doping levels, we establish that these two scales are associated with coherent excitations of the superconducting state which disappears at T_c. Using a simple model, we show that these two scales do not require the existence of two gaps. Rather, a single d-wave superconducting gap with a loss of Bogoliubov quasiparticle spectral weight in the antinodal region is shown to reconcile spectroscopic [9–17] and transport [18–21] measurements.

In panels a-b of Fig. 1, we display the Raman spectra $\chi''(\omega, T)$ of Bi-2212 samples with different doping levels in B_{1g} (antinodal) and B_{2g} (nodal) geometries (see Methods), for several temperatures ranging from well below T_c to 10 K above T_c. In both geometries, these spectra show the gradual emergence of a peak as the sample is cooled below T_c. An important observation is that the Raman responses at T_c and just above T_c are essentially identical. This suggests that the emergence of the B_{1g} and B_{2g} peaks below T_c is associated with coherent excitations of the superconducting state. The B_{1g} peak (measured at $T = 10$ K) is seen to decrease in intensity as the doping level is reduced, and disappears altogether at the lowest doping $p \simeq 0.1$. In contrast, the B_{2g} peak intensity remains sizeable even at low doping levels.

In order to clearly reveal the temperature-dependence of the B_{1g} and B_{2g} peaks, we have plotted the normalized areas of the B_{1g} and B_{2g} peaks in Fig.1e as a function of T/T_c. This plot demonstrates that the peak intensities vanish at T_c for all doping levels, providing quantitative support to our interpretation as coherence peaks of the superconducting state. The subtracted spectra displayed in Fig. 1c-d (see caption) allow for a quantitative determination of the characteristic energy scales associated with the superconducting coherence peaks (see plot in Fig. 1f). It is seen that the B_{1g} and B_{2g} energy scales track each other at high doping

levels ($p \gtrsim 0.19$), but depart from each other as doping is reduced. The B_{1g} energy scale increases monotonically as doping is reduced, while the B_{2g} energy scale follows a dome-like shape approximately similar to that of the critical temperature T_c.

In order to shed light on the origin of these two energy scales, we consider a very simple phenomenological model of a superconductor with a gap function $\Delta(\phi)$. The angle ϕ is defined by $\cos(2\phi) = \cos k_x - \cos k_y$ and the gap function vanishes at the nodal point $\Delta(\phi = \pi/4) = 0$ while it is maximal at the antinodes $\Delta(\phi = 0) = \Delta_{max}$. Within a Fermi liquid description, the quasiparticle contribution to the Raman response in the superconducting state reads [3, 11]:

$$\chi''_{B_{1g},B_{2g}}(\Omega) = \frac{2\pi N_F}{\Omega} \left\langle \gamma^2_{B_{1g},B_{2g}}(\phi)\, Z^2(\phi)\Lambda^2(\phi) \frac{\Delta(\phi)^2}{\sqrt{(\hbar\Omega)^2 - 4\Delta(\phi)^2}} \right\rangle_{FS} \quad (1)$$

In this expression, $\langle(\cdots)\rangle_{FS}$ denotes an angular average over the Fermi surface, $\gamma_{B_{1g},B_{2g}}$ are the Raman vertices which read $\gamma_{B_{1g}}(\phi) = \gamma^0_{B_{1g}} \cos 2\phi$ and $\gamma_{B_{2g}}(\phi) = \gamma^0_{B_{2g}} \sin 2\phi$, respectively. , and $\Delta(\phi)^2/\sqrt{\Omega^2 - 4\Delta(\phi)^2}$ is a BCS coherence factor. The function $Z(\phi)$ is the spectral weight of the Bogoliubov quasiparticles, while $\Lambda(\phi)$ is a Fermi liquid parameter associated with the coupling of these quasiparticles to the electromagnetic field.

In the following, we will show that the angular dependence of the quasiparticle renormalization, $Z.\Lambda(\phi)$, plays a key role in accounting for the experimental observations. In the B_{1g} geometry, the Raman vertex $\gamma_{B_{1g}}(\phi)$ is peaked at the antinode $\phi = 0$, resulting in a pair-breaking coherence peak at $\hbar\Omega_{B_{1g}} = 2\Delta_{max}$ due to the singularity of the BCS coherence factor. The weight of this peak is directly proportional to the antinodal quasiparticle renormalization $(Z\Lambda_{AN})^2 = (Z\Lambda)^2(\phi = 0)$. Hence, the fact that the B_{1g} coherence peak loses intensity at low doping strongly suggests that $Z\Lambda_{AN}$ decreases rapidly as doping is reduced, in qualitative agreement with tunneling [12, 13] and ARPES measurements [22, 23].

In the B_{2g} geometry, the situation is more subtle because the Raman vertex is largest at the nodes, where the BCS coherence factor vanishes. As a result, the energy of the coherence peak depends sensitively on the angular dependence of the quasiparticle renormalization $Z\Lambda(\phi)$. If the latter is approximately constant along the Fermi surface, then the energy of the B_{2g} peak is determined solely by the angular extension of the Raman vertex $\gamma_{B_{2g}}(\phi)$. In contrast, let us consider a $Z\Lambda(\phi)$ which varies significantly, from a larger value $Z\Lambda_N$ at the node to a small value $Z\Lambda_{AN}$ at the antinode, with a characteristic angular extension ϕ_N around the node, smaller than the intrinsic width of the Raman vertex $\gamma_{B_{2g}}(\phi)$. Then, it is

ϕ_N itself which controls the position of the B_{2g} peak: $\hbar\Omega_{B_{2g}} = 2\Delta(\phi_N)$. As shown below, this key feature explains the origin of the differentiation between the two energy scales in underdoped cuprates.

To proceed further in the simplest possible way, we consider a simple crenel-like shape for $Z\Lambda(\phi)$, varying rapidly from $Z\Lambda_N$ for $\phi_N < \phi < \pi/4$ to $Z\Lambda_{AN} < Z\Lambda_N$ for $0 < \phi < \phi_N$ (Fig. 2.AII-CII). Furthermore, we adopt the often-used [24] parametrization of the gap function $\Delta(\phi) = \Delta_{max}\ [B\cos 2\phi + (1-B)\cos 6\phi]$, consistent with d-wave symmetry where the nodal slope of the gap $v_\Delta \equiv \partial\Delta/\partial\phi|_{\phi=\pi/4} = 2(4B-3)\Delta_{max}$ does not necessarily track Δ_{max}.

We thus have 5 parameters: Δ_{max}, the nodal slope of the gap, v_Δ or B (see Methods), $Z\Lambda_{AN}$, $Z\Lambda_N$ and the angular extension ϕ_N. These parameters are determined by attempting a semi-quantitative fit to our spectra, obeying the following constraints:

- The maximum gap Δ_{max} is determined from the measured energy of the B_{1g} peak according to $2\Delta_{max} = \hbar\Omega_{B_{1g}}$
- The antinodal quasiparticle renormalization $Z\Lambda_{AN}$ is determined such as to reproduce the intensity of the B_{1g} coherence peak.
- The angular extension ϕ_N is determined from the energy of the nodal coherence peak. Throughout the underdoped regime, this amounts to $2\Delta(\phi_N) = \hbar\Omega_{B_{2g}}$ as discussed above.
- The nodal renormalization $Z\Lambda_N$ is constrained to insure that the ratio $(Z\Lambda_N)^2/v_\Delta$ does not change as a function of doping level, at least in the range $0.1 < p < 0.16$ (as shown in Refs. [3, 10]). This ratio controls the low-frequency slope of the B_{2g} Raman response. We assume here that the density of states N_F (associated with the Fermi velocity perpendicular to the Fermi surface) does not depend sensitively on doping level in this range.

These 4 constraints leave one parameter undetermined, which can be taken as the deviation of the gap function from a pure $\cos k_x - \cos k_y$ form, as measured by the ratio $v_\Delta/(2\Delta_{max}) = 4B - 3$ of the nodal velocity to the gap maximum. We will thus consider three possible scenarios:

- (A) Pure $\cos k_x - \cos k_y$ gap: $v_\Delta = 2\Delta_{max}$ $(B = 1)$. This corresponds to a superconducting gap involving a single characteristic energy, which increases as the doping level is reduced.

- (B) v_Δ tracks the critical temperature T_c. In this case, the gap function is truly characterized by two scales varying in opposite manner as the doping level is reduced.

- (C) v_Δ remains constant as a function of doping. This is also a two-scale superconducting gap scenario, although with a milder variation of v_Δ .

In Fig.2, we display the B_{1g} and B_{2g} Raman spectra calculated in the framework of this simple theoretical analysis, following each of the three scenarios (A-C) above. We observe that the main aspects of the experimental spectra, and most importantly *the existence of two energy scales* $\Omega_{B_{1g}}$, $\Omega_{B_{2g}}$ *varying in opposite manners as a function of doping*, can be reproduced within any of the three scenarios.

A common feature between all three scenarios is that the quasiparticle renormalization function $Z\Lambda(\phi)$ varies significantly along the Fermi surface. Quasiparticles have a large spectral weight $Z\Lambda_N$ only on a restricted region around the nodes, defined by ϕ_N, corresponding to a fraction $f_c \equiv (\pi/4 - \phi_N)/(\pi/4)$ of the Fermi surface. While Δ_{max} increases with falling doping, $\Delta(\phi_N)$ decreases because of the rapid contraction of the 'coherent fraction' f_c , leading to the opposite doping dependence of the two scales, as illustrated on Fig. 3a. We note that linearizing the gap function in the coherent region is a reasonable approximation for the A and C scenarios, leading to the relation $\hbar\Omega_{B_{2g}} = \frac{\pi}{2} f_c \, v_\Delta \propto k_B T_c$ which links the nodal (B_{2g}) energy scale (proportional to T_c), the nodal velocity and the coherent fraction. This approximation is not valid for scenario B, because linearization is not accurate there.

It is clear that having uniformly coherent Bogoliubov quasiparticles along the Fermi surface is inconsistent with our data, especially in view of the rapid suppression of the B_{1g} coherence peak and the corresponding decrease of $Z\Lambda_{AN}$. This is one of the key conclusions of the present work.

In panels (A.V-C.V) of Fig.2, we display a calculation of the corresponding tunneling conductance, (see Methods). One sees that the two energy scales have clear signatures in the tunneling spectra, the nodal (B_{2g}) one corresponding to a 'kink'-like feature. Such a feature has indeed been observed in tunneling spectra [6, 12, 17], although it has been usually interpreted as evidence that v_Δ and Δ_{max} are two distinct scales (scenarios B, or

C), without considering the effect of $Z(\phi)$. Our work demonstrates that the STM 'kink' results quite generally from the rapid decrease of the quasiparticle spectral weight as one moves from nodes to antinodes.

Although the above features are common to all three scenarios, there are two key differences between them. The first one is qualitative: in scenario A, $Z\Lambda_N$ *increases* as doping level is reduced, while it *decreases* for scenario B and stays constant for scenario C. The second, quantitative, difference is the rate at which the coherent fraction of the Fermi surface f_c decreases with underdoping, being largest for scenario A and smallest for B (Fig. 3b).

A determination of the coherent fraction ${f_c}^{HC}$ has been reported from heat-capacity (HC) measurements [18, 19], as reproduced on Fig. 3b. It was also reported from ARPES [14, 25] in the normal state, that the Fermi arcs shrink upon cooling as $\sim T/T^*$. The doping evolution of the coherent fraction ${f_c}^{ARPES} \propto T_c/T^*$ at T_c is displayed in Fig.3b. Remarkably, we find that there is a good *quantitative* agreement between the doping dependence of f_c reported from HC and ARPES and our determination from Raman within scenario A (a single gap scale $v_\Delta \propto \Delta_{max}$), which thus appears to be favored by this comparison. Although this quantitative agreement should perhaps not be overemphasized in view of the uncertainties associated with each of the experimental probes, we conclude that this single-gap scenario (A) stands out as the most likely possibility. Our interpretation also reconciles the distinct doping dependence of the two energy scales with thermal conductivity measurements in underdoped samples which, interpreted within the clean limit, suggest that $v_\Delta \propto \Delta_{max}$ [20, 21] (see, however [26]).

As noted before, with a single superconducting gap, the relation between the critical temperature (or $\Omega_{B_{2g}}$) and the coherent fraction reads: $k_B T_c \propto f_c \, \Delta_{max}$. We are then led to conclude that it is the suppressed coherence of the quasiparticles that sets the value of T_c, while Δ_{max} increases with underdoping. From our findings, we anticipate that the loss of coherent of Bogoliubov quasiparticles on a restricted part of the Fermi surface only is a general feature of how superconductivity emerges as holes are doped into a Mott insulating state.

METHODS

Details of the experimental procedure

The Bi-2212 and Hg-1201 single crystals have been grown by using a floating zone method and flux technique respectively. The detailed procedures of the crystal growth are described elsewhere [10, 27, 28]. The doping value p is inferred from T_c using equation of Presland et al from Ref. [29]: $1 - T_c/T_c^{max} = 82.6\,(p - 0.16)^2$. T_c has been determined from magnetic susceptibility measurements for each doping level. Raman experiments have been carried out using a triple grating spectrometer (JY-T64000) equipped with a nitrogen cooled CCD detector. All the measurements have been corrected for the Bose factor and the instrumental spectral response. The B_{1g} and B_{2g} geometries have been obtained using crossed light polarizations at 45^o from the $Cu-O$ bond directions and along them respectively. In these geometries we probe respectively, the antinodal (AN) and nodal (N) regions correponding to the principal axes and the diagonal of the Brillouin zone.

Calculation of the tunneling conductance

$\frac{dI}{dV} \propto N_F \left\langle Z(\phi)\,\mathrm{Re}\frac{\mathrm{eV}-\mathrm{i}\Gamma}{(\mathrm{eV}-\mathrm{i}\Gamma)^2-\Delta(\phi)^2}\right\rangle_{FS}$ where $\Gamma = \Delta_{max}\,/30$ is a small damping factor, and we have assumed for simplicity that $Z(\phi)$ and $Z\Lambda(\phi)$ can be identified.

ACKNOWLEDGEMENTS

We are grateful to J. Mesot, A. Yazdani, A. J. Millis, P. Monod and C. Ciuti for very helpful discussions. Correspondance and requests for materials should be addressed to A.S. (alain.sacuto@univ-paris-diderot.fr).

---

[1] Bardeen, J., Copper, L.N, & Schrieffer, J.R. Theory of superconductivity. *Phys.Rev.* **106**, 162 (1957).

[2] Deutscher,G. *et al.* Coherence and single-particle excitations in the high-temperature superconductors. *Nature* **397**,410 (1999).

[3] Le Tacon, M. *et al.* Two energy scales and two distinct quasiparticle dynamics in the superconducting state of underdoped cuprate. *Nature Phys.* **2**, 537 (2006).

[4] Tanaka, K. *et al.* Distinct Fermi-momentum-dependent energy gaps in deeply underdoped Bi2212. *Science* **314**, 1910 (2006).

[5] Lee, W. S. *et al.* Abrupt onset of a second energy gap at the superconducting transition of underdoped Bi-2212. *Nature* **450**, 81 (2007).

[6] Boyer, M. C. *et al.* Imaging the two gaps of the high-temperature superconductor $Bi_2Sr_2CuO_{6+x}$. *Nature Phys.* **3**, 802 (2007).

[7] Millis, A. Gaps and Our Understanding. *Science***314**, 1888 (2006).

[8] Hufner, S., Hossain, M. A., Damascelli, A. & Sawatzky, G. A. Two gaps make a high-temperature superconductor. *Rep. Prog. Phys.* **71**, 062501 (2008).

[9] Guyard, W.*et al.* Breakpoint in the evolution of the gap through the cuprate phase diagram. *Phys. Rev. B* **77**, 024524 (2008).

[10] Blanc, S. *et al.* Quantitative Raman measurement of the evolution of the Cooper-pair density with doping in $Bi_2Sr_2CaCu_2O_{8+\delta}$ superconductors. *Phys. Rev. B* **80**, 140502R (2009).

[11] Devereaux, T. P. & Hackl, R.Inelastic light scattering from correlated electrons *Rev. Mod. Phys.* **79**, 175 (2007).

[12] McElroy, K.*et al.* Coincidence of Checkerboard Charge Order and Antinodal State Decoherence in Strongly Underdoped Superconducting $Bi_2Sr_2CaCu_2O_{8+\delta}$. *Phys. Rev. Lett.* **94**, 197005 (2005).

[13] Kohsaka, Y. *et al.* How Cooper pairs vanish approaching the Mott insulator in $Bi_2Sr_2CaCu_2O_{8+\delta}$. *Nature* **454**, 28 (2008).

[14] Kanigel, A. *et al.* Protected Nodes and the Collapse of Fermi Arcs in High-Tc Cuprate Superconductors. *Phys. Rev. Lett.* **99**, 157001 (2007).

[15] Kondo, K., Khasanov, R., Takeuchi, T., Schmalian, J. & Kaminski, A. Competition between the pseudogap and superconductivity in the high-Tc copper oxides. *Nature* **457**, 296 (2009).

[16] Chatterjee, U. *et al.* Observation of a d-wave nodal liquid in highly underdoped $Bi_2Sr_2CaCu_2O_{8+\delta}$. *Nature Phys.* **5**, 1456 (2009).

[17] Pushp, A. *et al.* Extending Universal Nodal Excitations Optimizes Superconductivity in $Bi_2Sr_2CaCu_2O_{8+\delta}$. *Science* **26**, 1689 (2009).

[18] Wen, H.H. *et al.* Pseudogap, superconducting energy scale, and Fermi arcs of underdoped

cuprate superconductors. *Phys. Rev.B* **72**, 134507 (2005).

[19] Matsuzaki, T., Momono, N., Oda, M. & Ido,M. Electronic Specific Heat of $La_{2-x}Sr_xCuO_4$: Pseudogap Formation and Reduction of the Superconducting Condensation Energy*J. Phys. Soc. Jpn.* **73**, 2232 (2004).

[20] Sutherland, M.*et al.* Thermal conductivity across the phase diagram of cuprates: Low-energy quasiparticles and doping dependence of the superconducting gap. *Phys. Rev.B* **67**, 174520, (2003).

[21] Hawthorn, D.G *et al.* Doping dependence of the superconducting gap in $Tl_2Ba_2CuO_{6+\delta}$ from heat transport.*Phys. Rev. B* **75**, 104518 (2007).

[22] Ding, H. *et al.* Coherent Quasiparticle Weight and Its Connection to High-T_c Superconductivity from Angle-Resolved Photoemission, *Phys. Rev. Lett.* **87**, 227001 (2001).

[23] Vishik *et al.* A momentum-dependent perspective on quasiparticle interference in $Bi_2Sr_2CaCu_2O_{8+\delta}$ *Nature phys.* **5**, 718, (2009).

[24] Mesot, J. *et al.* Superconducting Gap Anisotropy and Quasiparticle Interactions: A Doping Dependent Photoemission Study. *Phys. Rev. Lett.* **83**, 840, (1999).

[25] Kanigel, A. *et al.* Evolution of the pseudogap from Fermi arcs to the nodal liquid. *Nature Phys.* **2**, 447 (2006).

[26] Sun, X. F. *et al.* Electronic Inhomogeneity and Breakdown of the Universal Thermal Conductivity of Cuprate Superconductors, *Phys. Rev. Lett.* **96**, 017008, (2006).

[27] Wen, J. S. *et al.* Large Bi-2212 single crystal growth by the floating-zone technique. *J. of Crystal Growth.* **310**, 1401 (2008).

[28] Bertinotti A. *et al.* In studies of High Temperature Superconductors Vol.**23** (ed. A. Narlikar), 27-85 (Nova Science Publishers New York, (1997).

[29] Presland M. R. *et al.* General trends in oxygen stoichiometry effects on Tc in Bi and Tl superconductors. *Physica C* **176**, 95 (1991).

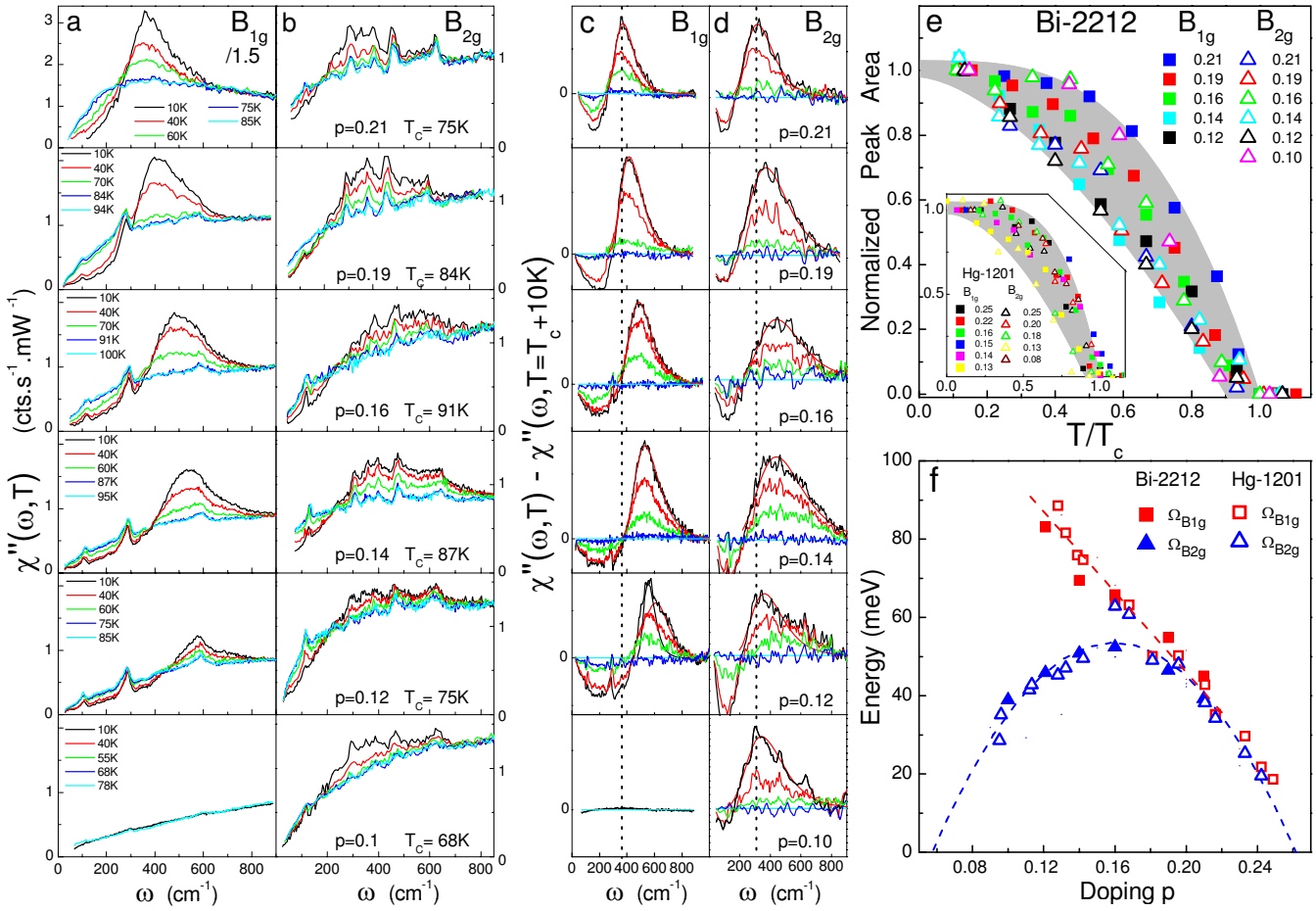

FIG. 1: (color online) **Temperature dependence of the Raman spectra.** **a**,**b**: Raman spectra, $\chi''(\omega, T)$ of Bi-2212 single crystals for several doping levels in B_{1g} (Antinodal) and B_{2g} (Nodal) geometries. **c**, **d**: Raman spectra subtracted from the one measured at 10 K above T_c for each sample in each geometry. A direct visual comparison of the subtracted spectra to a reference energy (chosen as the peak position for the most overdoped sample, drawn as a guide to the eyes) clearly reveals the distinct doping-dependence of these two energy scales. **e**: Temperature dependence of the normalized areas of the B_{1g} and B_{2g} peaks with respect to the area measured at $T = 10$ K. The inset displays these areas for Hg-1201 crystals. **f**: Energy scales associated to the B_{1g} and B_{2g} peaks for both Bi-2212 and Hg-1201 crystals. The dashed lines are guides to the eyes and track the locations of the superconducting peak maxima.

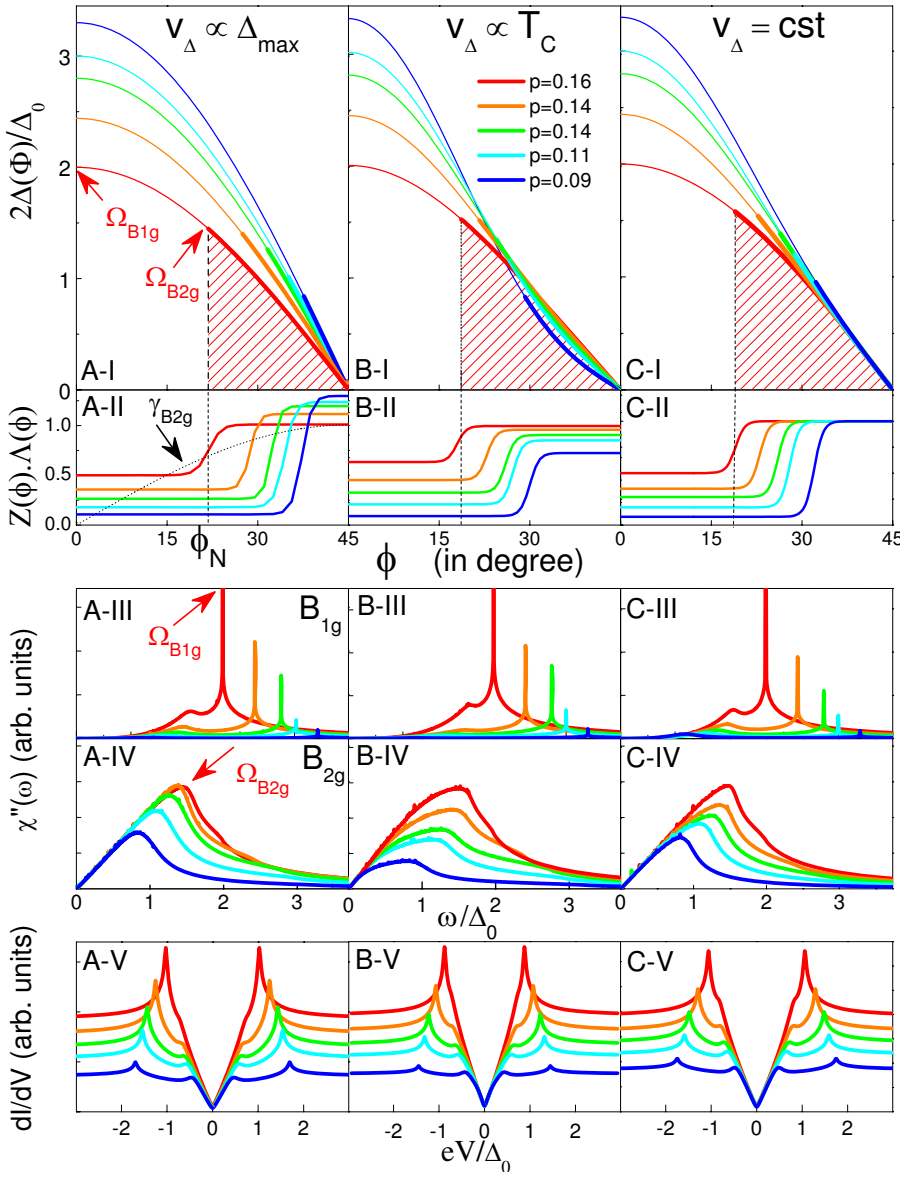

FIG. 2: (color online) **Three scenarios for underdoped cuprates. A.I-C.I**: Doping evolution of the superconducting gap in the three scenarios (A-C). **A.II-C.II**: Angular dependences of the quasiparticle spectral weights $Z\Lambda(\phi)$ as a function of doping level for each scenario. The angular dependence of the B_{2g} Raman vertex is shown in dotted line (see **AII**). **A.III-C.III, A.IV-C.IV**: Calculated Raman spectra for each scenario in B_{1g} and B_{2g} geometries. The locations of the B_{1g} and B_{2g} peaks are respectively controlled by the gap energy at the antinodes $\Phi = 0$ and at the angle Φ_N. Note that the low energy slope of the B_{2g} Raman response is constant with doping as observed experimentally [10]. **A.V-C.V**: Tunneling spectra for the three scenarios.

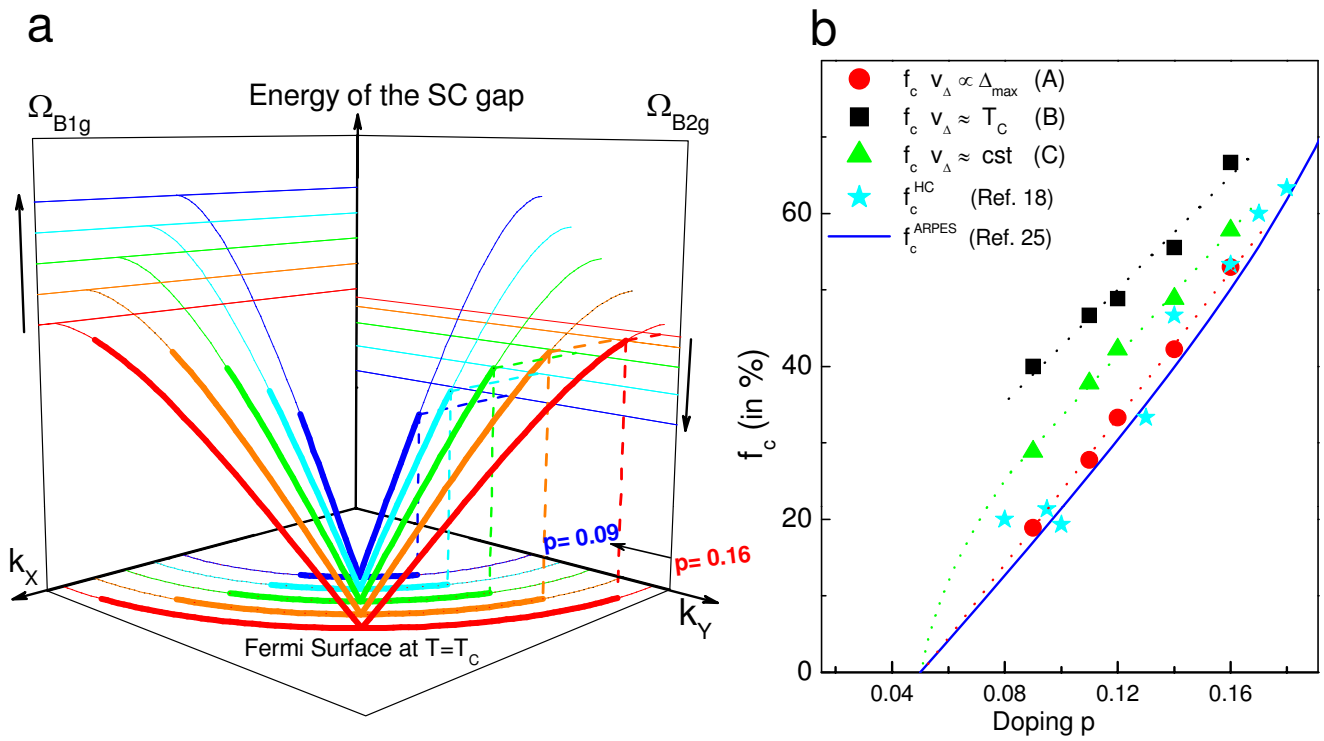

FIG. 3: (color online) **Fermi surface coherent fraction and a single d-wave superconducting gap.** **a**: Scenario A where coherent Bogoliubov quasiparticles are partially suppressed on restricted parts of the Fermi surface and the superconducting gap has a single d-wave shape. **b**: Doping evolution of the coherent fraction of the Fermi surface (f_c) in the three scenarios (A-C). The ${f_c}^{ARPES}$ curve is deduced from $L_{arc}/L_{full}(T_c) = 1 - 0.70\frac{T_c}{T^*}$ (see Ref.[25]), expressed as a function of the doping level. ${f_c}^{HC}$ is extracted from the zero temperature specific heat coefficient $\gamma(0)_n$, [18, 19].